Analysis and Model-Based Control of Servomechanisms With Friction

Evangelos G. Papadopoulos
e-mail: egpapado@central.ntua.gr

Georgios C. Chasparis
e-mail: gchas@seas.ucla.edu
Department of Mechanical Engineering, National Technical University of Athens, 15780 Athens, Greece

Friction is responsible for several servomechanism limitations, and their elimination is always a challenge for control engineers. In this paper, model-based feedback compensation is studied for servomechanism tracking tasks. Several kinetic friction models are employed and their parameters identified experimentally. The effects of friction compensation on system response are examined using describing function analysis. A number of control laws including classical laws, rigid body motion models, and friction compensation are compared experimentally in large-displacement tasks. Results show that the best response is obtained using a controller that incorporates a rigid body model and a friction model based on an accurate description of identified kinetic friction effects. [DOI: 10.1115/1.1849245]

1 Introduction

Friction is one of the most important limitations in high-precision positioning systems. It can cause tracking errors, and may result in limit cycles. Armstrong-Helouvry et al. [1] have presented methods for friction compensation proposed in the past including feedback and feedforward compensation. These methods rely upon a friction model and exact knowledge of its parameters, making friction identification necessary.

Off-line identification of friction is described by Armstrong [2], and Popovic et al., [3]. In [2], a very simple technique is suggested in which static friction is measured by a number of breakaway experiments. This technique is applied to a complex mechanism, with the addition of measuring the static friction as a function of position [3]. To find the friction–velocity relationship, several constant velocity motions were used [3]. On the other hand, on-line identification methods are used usually in conjunction with adaptive control schemes, Friedland [4].

Many friction models have been proposed that differ on the friction effects that are modeled in a lubricated contact. Examples of kinetic friction models, where friction force is a function of velocity, are given in [1] or also those given by Olsson et al. in [5], Karnopp in [6] and Altpeter et al. in [7]. State or dynamic friction models, which embody the natural mechanism of friction generation, are introduced in [1] and [5]. Kinetic friction models, such as the classical or the general kinetic friction models, are simpler than dynamic friction models [1,5,7], they tend to be sufficient for large displacement tasks, and they do not require large computing power [7].

Even if friction is modeled with high accuracy, there always may be a slight mismatch that may affect tracking accuracy or cause adverse oscillations. Therefore, the effect of this mismatch on system response must be studied. Several analysis methods have been applied, such as the phase-plane analysis, [1], and Radcliffe et al. [8], the algebraic analysis, Armstrong-Helouvry et al. [9], and the Single-Input Describing Function (SIDF) analysis, [1,10–13]. SIDF analysis is among the basic tools for analyzing systems with friction, and can be applied in two different techniques, the memoryless element construction and the integrated friction/plant construction [1,10].

Limit cycles, caused by Coulomb friction in a drive motor without friction compensation, are related to the stability of the regulator; see Wallenborg et al. [11]. These results have been also verified in the case of PID control and Coulomb friction by Armstrong-Helouvry [12]. The conditions needed to avoid limit cycles resulting from overcompensation when Coulomb friction is used as the basis for friction compensation were examined by Canudas de Wit et al. in [13], where a control scheme is also proposed for reducing amplitude and modifying frequency of oscillations caused by friction overcompensation.

In this paper, a combination of rigid-body and friction models in controlling a servomechanism is studied aiming at improving its tracking response. Friction models such as the classical friction model, the general kinetic friction model and a properly modified kinetic friction model, which better describes observed kinetic friction anomalies in servomechanisms, are studied. Kinetic friction model parameters are identified experimentally for all models as a function of position and velocity. SIDF analysis is employed to predict limit cycle generation in the case of PD control due to friction compensation. Design guidelines on the use of friction compensation are established, that apply even to more complicated kinetic friction models than the classical ones, such as the proposed modified kinetic friction model. Friction compensation is employed in servo large-displacement tracking tasks. A number of classical, model-based, and friction compensating control laws are implemented using the studied friction models and compared experimentally. Results show that the best response is obtained using a controller that includes a rigid body model and friction compensation employing the proposed modified kinetic friction model.

2 Basic Friction Models

Kinetic friction models, also called static friction models, or steady-state friction models, compute friction torque as a function of a slowly varying velocity. The classical friction model or the Coulomb-plus-Viscous (CV) friction model is described by

$$T_f = T_C \operatorname{sgn} \dot{\theta} + b\dot{\theta} \tag{1}$$

where T_C is the Coulomb friction torque and b is the viscous friction coefficient.

If static (stick) friction is added to Eq. (1), the classical friction model is complete. During stick, the friction force is modeled as a function of the external force acting on a mass. Thus, the *complete classical friction model or the Static-plus-Coulomb-plus-Viscous (SCV) friction model*, see Fig. 1(*a*), is described by

$$T_f = \begin{cases} T_C \operatorname{sgn} \dot{\theta} + b\dot{\theta}, & \dot{\theta} \neq 0 \\ T_e, & |T_e| < T_s,\ \dot{\theta} = 0,\ \ddot{\theta} = 0 \\ T_s \operatorname{sgn} T_e, & |T_e| > T_s,\ \dot{\theta} = 0,\ \ddot{\theta} \neq 0 \end{cases} \tag{2}$$

where T_e is the external torque, and T_s is the breakaway torque, which characterizes the limit between the static friction regime and the kinetic friction regime.

More accurate friction modeling at very low velocities has shown that the friction torque which rises from the breakaway level, T_s, to the Coulomb level, T_C, is not discontinuous, but is a function of velocity [1]. This continuous dependence of friction on velocity, called the *Stribeck curve* or the *General Kinetic (GK) friction model*, see Fig. 1(*b*), is described by

Contributed by the Dynamic Systems, Measurement, and Control Division of THE AMERICAN SOCIETY OF MECHANICAL ENGINEERS for publication in the ASME JOURNAL OF DYNAMIC SYSTEMS, MEASUREMENT, AND CONTROL. Manuscript received November 29, 2004; final revision, March 25, 2004. Review conducted by: J. Tu.

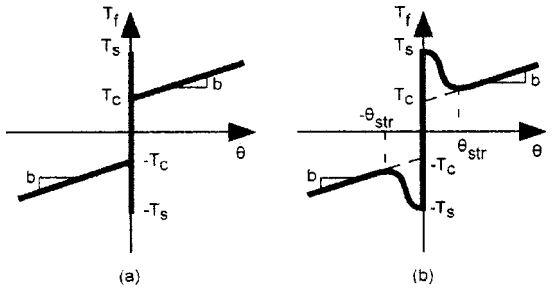

Fig. 1 (*a*) The Static-plus-Coulomb-plus-Viscous (SCV) friction model; (*b*) The General Kinetic Friction (GK) model

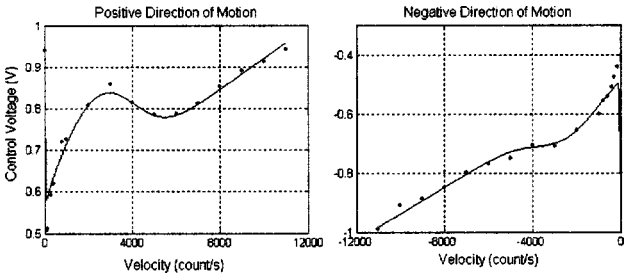

Fig. 3 Position-mean control voltage for several constant velocities and for the two directions of motion

$$T_f = \begin{cases} (T_C + (T_s - T_C)\exp(-|\dot{\theta}/\dot{\theta}_{Str}|^2)\cdot \operatorname{sgn}\dot{\theta} + b\dot{\theta}, & \dot{\theta} \neq 0 \\ T_e, \quad |T_e| < T_s, & \dot{\theta} = 0, \ \ddot{\theta} = 0 \\ T_s \operatorname{sgn} T_e, \quad |T_e| > T_s, & \dot{\theta} = 0, \ \ddot{\theta} \neq 0 \end{cases} \tag{3}$$

where $\dot{\theta}_{Str}$ is the Stribeck velocity. The problem of defining zero velocity has been pointed out by Karnopp, [6], who introduced an interval in which the velocity can be considered as zero, thus avoiding the switching between sticking and sliding.

3 System Configuration and Modeling

To be able to test experimentally control laws in the presence of friction, an experimental servomechanism device is used. Motion is achieved by means of a roller-screw driver with a fixed centered carriage, as shown in Fig. 2(*a*). The driver uses a 48 V, 70 W dc motor with a torque constant of $K_T = 0.105$ Nm/A, driven by a PWM amplifier running in current mode with gain $K_{amp} = 0.4$ A/V. The motor is equipped with a $K_{enc} = 500$ count/rev $= 79.6$ count/rad incremental encoder resulting in a 0.001 26 rad rotor angular accuracy, or, equivalently, in a 42 μm carriage positional resolution. To avoid differentiation problems in estimating angular velocity, a small dc motor with a back-emf constant $K_{gen} = 4.46 \times 10^{-3}$ V s/rad, is used as a tachometer feeding back screw angular velocity, filtered by a 4 Hz low pass filter. A motion controller card (GALIL DMC-1700) reads the encoder and tachometer signals. This card is interfaced to a 500 MHz Pentium III PC, running the QNX real-time operating system. The experimental device is shown schematically in Fig. 2(*b*).

The servomechanism is governed by the following rigid body dynamics

$$J\ddot{\theta} = T_m - T_f \tag{4}$$

where J is the equivalent (total) rotor-reflected inertia, θ is the angular rotor displacement, T_f is the friction torque, and T_m is the motor torque, which is given by

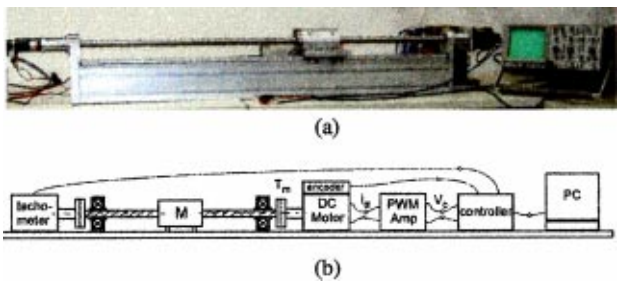

Fig. 2 (*a*) Servomechanism experimental setup including sensors, amplifier, and controller; (*b*) system schematic

$$T_m = K_T i_a = K_T K_{amp} V_c \tag{5}$$

where i_a is the amplifier output current, and V_c is the amplifier control voltage.

4 Servomechanism Friction Identification

In order to identify friction for the servomechanism described above, two distinct experiments were designed. The first yields the breakaway friction torque, while the second yields the kinetic friction parameters. The experiments were run in an automated and unattended fashion during servomechanism idling time. This feature allows for controller optimization during actual system operation and can be used to improve performance at any time.

In the first experiment, the carriage is positioned at the one side of the roller-screw driver. Via a control program, the control voltage is increased gradually at the rate of 0.01 V/ms. When the encoder reads a very small displacement (set at 10 encoder counts) the position and breakaway control voltage are recorded. After the carriage comes to a rest for 20 s, a new experiment is initiated.

In the second experiment, the control voltage of the amplifier (equivalent to the friction level) for a constant carriage velocity is measured as a function of carriage position. The constant velocity is achieved with a plain PD controller and the experiment is repeated for several constant velocities.

The position-mean control voltage along the driver for several constant velocities and for the two directions of motion is displayed in Fig. 3. The zero-velocity control voltages are obtained by the first experiment, while the non-zero-velocity control voltages are obtained by the second experiment. As displayed in Fig. 3, a friction anomaly was observed at velocities below 6000 count/s, probably due to small bearing misalignment. Since such anomalies cannot be described by existing models and can be identified only by experiments on specific drives, one cannot use existing models blindly. However, the on-line approach used here, employed periodically, allows for the development of an accurate model, even if this model evolves with time.

The experimental results shown in Fig. 3 can be curve-fitted to an appropriate function. The curve-fitted function is enhanced by the inclusion of the exponential rise of friction at very low velocities, (Stribeck effect [1]), that is not reflected adequately in the experimental measurements in Fig. 3. This is due to the inability to achieve extremely low velocities because of low sensor accuracy. With these observations, the experimental points in Fig. 3, with the addition of static friction, yield the following kinetic friction model,

$$T_f=\begin{cases}[T_C+(T_s-T_C)\exp(-|\dot\theta/\dot\theta_{Str}|^2)+r|\dot\theta/\dot\theta_0|^{k_1}\exp(-|\dot\theta/\dot\theta_0|^{k_2})]\cdot\operatorname{sgn}\dot\theta+b\dot\theta, & \dot\theta\neq 0\\ T_e, \quad |T_e|<T_s, \quad \dot\theta=0, \quad \ddot\theta=0 & \\ T_s\operatorname{sgn}T_e, \quad |T_e|>T_s, \quad \dot\theta=0, \quad \ddot\theta\neq 0 & \end{cases} \tag{6}$$

where r, $\dot\theta_0$, k_1, k_2 are parameters to be determined. Equation (6) modifies the GK model by adding an additional exponential term that can describe servomechanism friction anomalies, and for this reason it is called the *Modified Kinetic (MK) friction model*.

Fitting the MK friction model for the two directions of motion to the experimental data resulted in the continuous lines in Fig. 3. Plots, such as the one in Fig. 3, were obtained for a number of closely located carriage positions, by measuring control voltages (currents) when the carriage is passing through the position of interest. By curve-fitting the experimental points, with the MK friction model for $\dot\theta\neq 0$, Eq. (6), we can estimate the friction parameters for all models, including the MK model and the basic friction models described in Sec. 2. The mean values of the above friction parameters are given in Table 1.

Finally, the effective inertia of the system is estimated from Eq. (4). Ten transient step response experiments were executed during which the velocity was recorded. Calculating the friction force from Eq. (6) and the acceleration by differentiating velocity, the rotor reflected system inertia was estimated as

$$J=1.58\times 10^{-4}\ \ \mathrm{Kg\,m^2} \tag{7}$$

5 Limit Cycle Analysis and Prediction

Even if friction identification aims at an accurate estimation of structural and parametric friction, there will always be some mismatch between estimated and plant friction. For this reason, before using estimated friction as compensation for plant friction, the effects of such compensation on a closed-loop system must be analyzed. To this end, a SIDF analysis is employed.

Figure 4 depicts the block diagram of a typical closed-loop servomechanism system, where system feedback consists of a state-feedback (PD) part and of an on-line friction compensation term, $\hat T_f$, which compensates for the plant friction, T_f. According to Sec. 4, plant friction is a function of current position and velocity. However, to simplify SIDF analysis, both T_f and $\hat T_f$ are considered functions of velocity only.

In order for SIDF to be applied, both T_f and $\hat T_f$ must be described analytically by some model. This enables us to reproduce the conditions responsible for limit cycle generation, such as a slight mismatch between T_f and $\hat T_f$. Since we are dealing with large-displacement tasks, we assume that both plant friction and friction compensation are described by a kinetic friction model [14].

Let $N(X)$, $\hat N(X)$ be the describing functions of the plant friction model and the friction compensation model, respectively. The closed-loop characteristic equation of the block diagram shown in Fig. 4 has the form

$$Js^2+[\Delta b+\Delta N(X)+K_dK_{amp}K_T]s+K_pK_{amp}K_T=0 \tag{8}$$

with

$$\Delta N(X)=N(X)-\hat N(X), \quad \Delta b=b-\hat b \tag{9}$$

Applying the memoryless element construction, see [1], the nonlinear part of the characteristic equation is separated from the linear part to yield

$$-\frac{1}{\Delta N(X)}=\frac{s}{Js^2+(\Delta b+K_dK_{amp}K_T)s+K_pK_{amp}K_T}=G_L(s) \tag{10}$$

If Eq. (10) is satisfied for some oscillation frequency ω and some amplitude X, then a limit cycle will occur. Replacing s with $j\omega$, and separating the real and imaginary parts, yields

$$\begin{aligned}\Delta N(X)&=-(\Delta b+K_dK_{amp}K_T)\\ \omega&=\sqrt{\frac{K_pK_{amp}K_T}{J}}\end{aligned} \tag{11}$$

A limit cycle will be generated if and only if

$$\begin{aligned}\operatorname{sgn}\{\Delta N(X)\}&=\operatorname{sgn}\{-(\Delta b+K_dK_{amp}K_T)\}\\ &\Leftrightarrow \Delta N(X)\cdot(\Delta b+K_dK_{amp}K_T)<0\end{aligned} \tag{12}$$

Since the MK friction model, Eq. (6), predicts well the experimental results, we assume that this model describes true plant friction, while for the friction compensation the CV friction model is used, Eq. (1). In this case, $\Delta N(X)$ takes the form

$$\Delta N(X)=\frac{4}{\pi X}\Delta T_C+\frac{2}{\pi X}(T_s-T_C)I_a(X)+\frac{2}{\pi X}rI_b(X) \tag{13}$$

where $\Delta T_C=T_C-\hat T_C$, $\hat T_C$ is the Coulomb friction level of the friction compensation term and $I_a(X)$, $I_b(X)$ are positive functions of X, see [15], that are given by

$$I_a(X)=\int_0^{\pi}\exp\left(-\left|\frac{X\sin\omega t}{\dot\theta_{Str}}\right|^2\right)\sin\omega t\,\mathrm{d}(\omega t) \tag{14}$$

Table 1 Mean values of friction parameters

Friction parameters	Mean Values		
	Positive direction	Negative direction	Multidirectional motion
T_s (Nm)	3.95e-2	3.37e-2	3.66e-2
T_C (Nm)	2.31e-2	2.01e-2	2.16e-2
$\dot\theta_{Str}$ (rad/s)	3.93e-1	1.23	8.12e-1
b (Nm s/rad)	1.26e-4	1.41e-4	1.34e-4
r (Nm)	1.50e-2	5.86e-3	1.04e-2
$\dot\theta_0$ (rad/s)	48.3	54.8	51.6
k_1	6.70e-1	1.27	9.70e-1
k_2	3.14	2.86	3.00

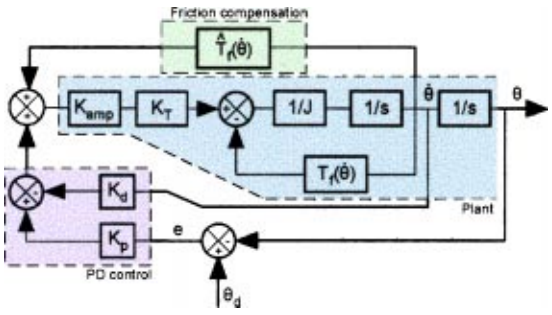

Fig. 4 Block diagram of the system with friction compensation and PD control

Table 2 Limit cycle generation map for friction described by the MK model and friction compensation by the CV model

	$\Delta b>0$	$\Delta b<0$
$\Delta T_C>0$	Never	If $0<K_d<-\dfrac{\Delta b}{K_{amp}K_T}$
$\Delta T_C<0$	If $0<P<-2\,\Delta T_C$	If $\begin{cases} 0<P<-2\Delta T_C \\ K_d>-\dfrac{\Delta b}{K_{amp}K_T}>0 \end{cases}$ or if $\begin{cases} P>-2\Delta T_C>0 \\ 0<K_d<-\dfrac{\Delta b}{K_{amp}K_T} \end{cases}$

$$I_b(X)=\int_0^{\pi}\left|\frac{X\sin\omega t}{\dot\theta_0}\right|^{k_1}\exp\left(-\left|\frac{X\sin\omega t}{\dot\theta_0}\right|^{k_2}\right)\sin\omega t\,\mathrm{d}(\omega t)$$

Thus, Eq. (12) is written as

$$\frac{2}{\pi X}[2\Delta T_C+(T_s-T_C)I_a(X)+rI_b(X)]\cdot(\Delta b+K_dK_{amp}K_T)<0 \tag{15}$$

Since

$$P(X)=(T_s-T_C)I_a(X)+rI_b(X)>0,\quad \text{and}\quad X,K_d>0 \tag{16}$$

the limit cycle generation map given in Table 2 is derived.

Similar guidelines can be derived if different kinetic friction models for both T_f and $\hat T_f$ are selected. In addition, one can point out that according to the Routh-Hurwitz stability criterion, the same closed loop system but without the nonlinearity of friction, is unstable when $\Delta b+K_dK_{amp}K_T<0$.

Thus, it is concluded that if there is no compensation for Coulomb friction or if there is compensation with $2\,\Delta T_C+P>0$, a limit cycle will be generated if and only if the system without the nonlinear part of friction is unstable. This result applies not only in the presence of plant friction, as suggested in Refs. [11] and [12], but *also* in the presence of friction compensation terms, as shown in this work.

The above limit cycle generation map does not contain the static friction regime, which is part of the plant friction. So, we must assume that the carriage will move (a limit cycle will occur) as long as the exercised torque is equal or larger than the breakaway torque, i.e.,

$$T_e\geqslant T_f=\begin{cases} T_s, & \text{if } \dot\theta=0,\ \ddot\theta=0 \\ T_C, & \text{if } \dot\theta=0,\ \ddot\theta\neq 0 \end{cases} \tag{17}$$

However, this condition does not influence the amplitude and the frequency of the limit cycle, because during a limit cycle, $\ddot\theta\neq 0$.

The qualitative and quantitative validity of these results has been studied through extensive simulations and experiments discussed in [15] and [16]. The results showed that the map generation of Table 2 in conjunction to Eq. (17) predicts satisfactorily the occurrence of a limit cycle. On the other hand, the amplitude and the frequency of a limit cycle can be given accurately by Eq. (11) under certain conditions, while a criterion for accurate quantitative results has been established.

6 Model-Based Control With Friction Models

Having the friction models and their experimentally obtained position-dependent parameters, see Sec. 4, various control laws are implemented and evaluated for tracking response tasks, where friction parameters are functions of the carriage position and such that limit cycles would never occur. The first model employed is the CV friction model, given by Eq. (1), in which velocities less than $\Delta\dot\theta=50$ count/s$=62.8$ rad/s are taken to be zero,

$$\hat T_{f,cv}(\theta,\dot\theta)=\hat T_C f(\dot\theta)+\hat b\,\dot\theta,\quad f(\dot\theta)=\begin{cases} +1, & \dot\theta>\Delta\dot\theta \\ 0, & |\dot\theta|\leqslant\Delta\dot\theta \\ -1, & \dot\theta<-\Delta\dot\theta \end{cases} \tag{18}$$

The second is the GK friction model, given by Eq. (3), without the static friction regime,

$$\hat T_{f,gk}(\theta,\dot\theta)=[\hat T_C+(\hat T_s-\hat T_C)\exp(-|\dot\theta/\hat\theta_{Str}|^2)]f(\dot\theta)+\hat b\,\dot\theta \tag{19}$$

and the third is the MK friction model, given by Eq. (6), without the static friction regime,

$$\hat T_{f,mk}(\theta,\dot\theta)=[\hat T_C+(\hat T_s-\hat T_C)\exp(-|\dot\theta/\hat\theta_{Str}|^2)+\hat r|\dot\theta/\hat\theta_0|^{\hat k_1}\exp(-|\dot\theta/\hat\theta_0|^{\hat k_2})]\cdot f(\dot\theta)+\hat b\,\dot\theta \tag{20}$$

In order to examine the tracking error response with friction compensation, several control schemes were employed. The trajectory was based on a triangular velocity profile. Except for the PD and PID, the other laws include estimates of the carriage inertia and of the resulting inertia forces to improve the tracking response without the use of large control gains.

- *Proportional-Derivative/state feedback* (PD),

$$T_{PD}=K_p(\theta_d-\theta)-K_d\dot\theta=K_pe-K_d\dot\theta \tag{21}$$

- *Proportional-Derivative-Integral* (PID),

$$T_{PID}=K_pe+K_d\dot e+K_i\int_0^t e(t)\,dt \tag{22}$$

- *Model-Based Control* (MB),

$$T_{MB}=\hat J\ddot\theta_d+K_d(\dot\theta_d-\dot\theta)+K_p(\theta_d-\theta)=\hat J\ddot\theta_d+K_d\dot e+K_pe \tag{23}$$

- *MB with the CV* friction model compensation given by Eq. (18) (MBCV),

$$T_{MBCV}=T_{MB}+\hat T_{f,cv} \tag{24}$$

- *MB with the GK* friction model compensation given by Eq. (19) (MBGK),

$$T_{MBGK}=T_{MB}+\hat T_{f,GK} \tag{25}$$

- *MB with the MK* friction model compensation given by Eq. (20) (MBMK),

$$T_{\mathrm{MBMK}}=T_{MB}+\hat T_{f,MK} \tag{26}$$

The closed-loop system block diagram for the various model-based schemes is shown in Fig. 5.

The PD, MB, MBCV, MBGK, and MBMK laws were run under QNX. The gains K_p, K_d were chosen for critical closed-loop damping, and for a frequency equal to 20.6 rad/s, assuming that friction is perfectly compensated. The PID control was executed by a loop implemented on the motion controller card. The PD and PID gains were chosen so that their resulting bandwidth and control voltages are at the same level with those of the other controllers.

Typical tracking errors and control voltages are displayed in Fig. 6. As shown in this figure, the PD law results in excessive tracking errors, as expected. The PID law tracking error was of the order of 20 counts and shows poor tracking during the acceleration and deceleration phases. However, due to its integral action, it drives the steady-state error to ± 1 counts.

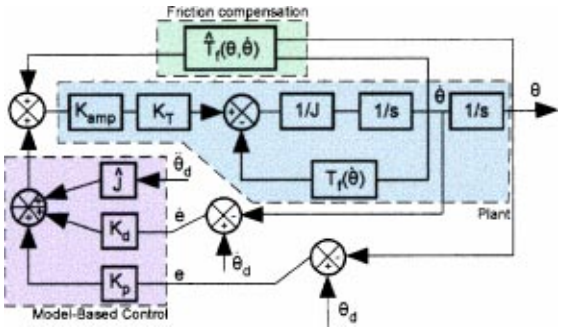

Fig. 5 Block diagram of the system with Model-Based Control and friction compensation

The MBMK law is better in comparison to the MBGK and MBCV laws, as shown in Fig. 6. This law reduces the tracking error below 10 counts throughout the motion. Therefore, its performance is ten times better than the PDs. Although these laws include no integral action, they exhibit very good performance, even at the steady state.

The experiments described above show that the use of a specific kinetic friction model describing special friction characteristics, such as the MK, reduces the tracking error considerably. Therefore, the use of an accurate friction model or of a look-up table specific to a given servomechanism is advantageous. However, this study revealed that although an accurate friction model such as the MK is advantageous, the inclusion of the rotor reflected system inertia and associated dynamics in the feedback control law was proved to be necessary, as well. Moreover, undesirable limit cycles can be eliminated by the proper choice of friction parameters. The fact that all the laws considered do not require additional feedback sensors or hardware but only additional software components, makes them attractive for improving system response beyond the response that is obtained by standard motion control cards.

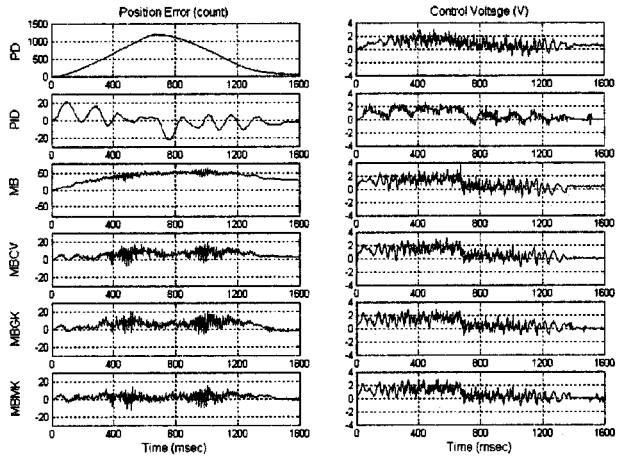

Fig. 6 Typical tracking error responses and respective control voltages

7 Conclusions

In this paper, the classical friction model, the general kinetic friction model, and a properly modified kinetic friction model, which better describes observed servomechanism kinetic friction effects, were used for reducing steady-state and tracking errors. Kinetic friction parameters were identified experimentally as a function of the current position and velocity during the system idle time. SIDF analysis was employed to predict limit cycle generation due to friction compensation, and guidelines on the use of friction compensation were established, even if more complicated kinetic friction models than the classical ones are used, such as the proposed modified kinetic friction model. Friction compensation was employed in servo large-displacement tracking tasks. A number of classical, model-based and friction compensating control laws were implemented and compared experimentally. Results showed that for both types of commands, a model-based control law with friction compensation based on a specifically modified kinetic friction model gave the best response. These results confirmed that using both inertia and friction models can improve the response of a servomechanism beyond the one obtainable by a standard motion control card.

References

[1] Armstrong-Helouvry, B., Dupont, P., and Canudas de Wit, C., 1994, ''A Survey of Models, Analysis Tools and Compensation Methods for the Control of Machines With Friction,'' Automatica, **30**, pp. 1083–1138.

[2] Armstrong, B., 1991, *Control of Machines with Friction*, Kluwer Academic Publishers, Boston, MA.

[3] Popovic, M. R., and Goldenberg, A. A., 1999, ''Friction Diagnostics and Modeling Using DFT Analysis,'' *Proc. of 1997 IEEE Conference on Robotics and Automation*, Albuquerque, NM, pp. 1669–1674.

[4] Friedland, B., Mentzelopoulou, S., and Park, Y. J., 1993, ''Friction Estimation in Multimass Systems,'' *Proc. of the 1993 American Control Conference*, San Francisco, CA, Vol. 2, pp. 1927–1931.

[5] Olsson, H., Aström, K. J., Canudas de Wit, C., Gafvert, M., and Lischinsky, P., 1998, ''Friction Models and Friction Compensation,'' J. Eur. Control, **4**, pp. 176–195.

[6] Karnopp, D., 1985, ''Computer Simulation of Stick-Slip Friction in Mechanical Dynamic Systems,'' ASME J. Dyn. Syst., Meas. Control, **107**, pp. 100–103.

[7] Altpeter, F., Ghorbel, F., and Longchamp, R., 1998, ''Relationship Between Two Friction Models: A Singular Perturbation Approach,'' *Proc. of 37th IEEE Conference on Decision & Control*, Tampa, FL, pp. 1572–1574.

[8] Radcliffe, C. J., and Southward, S. C., 1990, ''A Property of Stick-Slip Friction Models Which Promotes Limit Cycle Generation,'' *Proc. of the American Control Conference*, Vol. 2, pp. 1198–1203.

[9] Armstrong-Helouvry, B., and Amin, B., 1996, ''PID Control in the Presence of Static Friction: A Comparison of Algebraic and Describing Function Analysis,'' Automatica, **32**, pp. 679–692.

[10] Armstrong-Helouvry, B., and Amin, B., 1993, ''PID Control in the Presence of Static Friction, Part II: The Reliability of Describing Function Predictions,'' Technical Report, Dept. of Electrical Engineering and Computer Science, University of Wisconsin—Milwaukee, Report No. EE-93-2.

[11] Wallenborg, A., and Aström, K. J., 1988, ''Limit Cycle Oscillations in High Performance Robot Drives,'' *Proc. of IEEE International Conference CONTROL '88*, pp. 444–449.

[12] Armstrong-Helouvry, B., and Amin, B., 1994, ''PID Control in the Presence of Static Friction: Exact and Describing Function Analysis,'' *Proc. of the American Control Conference*, Baltimore, MD.

[13] Canudas de Wit, C., 1993, ''Robust Control for Servo-Mechanism Under Inexact Friction Compensation,'' Automatica, **29**, pp. 757–761.

[14] Ogata, K., 1970, *Modern Control Engineering*, Prentice–Hall, Englewood Cliffs, NJ.

[15] Chasparis, G., ''Design of a Servomechanism Control System With Friction Compensation,'' Master's Thesis, Department of Mechanical Engineering, Athens, Greece, 2001 (in Greek).

[16] Papadopoulos, E., and Chasparis, G., ''Analysis and Model-Based Control of Servomechanisms With Friction,'' *Proc. of the 2002 IEEE/RSG Int. Conference on Intelligent Robots and Systems (IROS '02)*, Lausanne, Switzerland, October 2002.